JOC*Article*

A Theoretical Study of the Competitive Homolytic/Heterolytic Aniomesolytic Cleavages of C−O Alkyl Ether Bonds

Xavier Asensio, Àngels González-Lafont, Jordi Marquet, and José M. Lluch*

Departament de Química, Universitat Autònoma de Barcelona, 08193 Bellaterra, Barcelona, Spain

lluch@klingon.uab.es

Received June 4, 2004

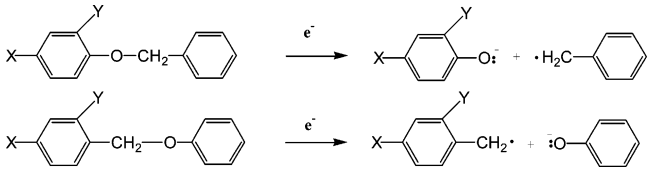

Density functional theory electronic structure calculations of the homolytic/heterolytic aniomesolytic C−O fragmentations in the gas phase of a series of radical anions of substituted-phenyl benzyl ethers and substituted-benzyl phenyl ethers have been carried out. Along the series, the electron-withdrawing strength of the substituents increases. An intramolecular electron transfer from the π system to the σ^* molecular orbital of the scissile C−O bond is required to produce the fragmentation. As the electron-withdrawing strength of the substituents increases, the transition-state structures appear later with higher potential energy and Gibbs free energy barriers. The homolytic mesolytic cleavages are always thermodynamically favored versus the corresponding heterolytic mesolytic ones. The heterolytic mesolytic fragmentations in radical anions containing only weak electron-withdrawing groups are faster than the corresponding homolytic mesolytic ones. Conversely, in radical anions supporting strong electron-withdrawing groups the homolytic mesolytic fragmentations are faster in terms of potential energy barriers. However, the entropic contribution makes it comparable the homolytic and the heterolytic Gibbs free energy barriers in this case. The main factors that determine the relative rates of those kind of aniomesolytic cleavages are discussed.

1. Introduction

The addition of an electron to a substrate often changes its reactivity dramatically.[1−4] So, activation induced by electron transfer consists of rendering a substrate reactive which, under the same conditions of temperature, pressure, and medium, would have been inert. The term dissociative activation is used for cases where addition or removal of an electron increases the tendency toward bond cleavage. Unimolecular fragmentation of radical anions to yield radicals and anions (aniomesolytic cleavages) constitutes an elementary step of many electron-transfer-initiated processes of chemical and biochemical interest.[5−9]

The most widely illustrated reactivity in the chemistry of organic radical anions is probably the dissociative activation, with respect to their corresponding neutral species, of σ^* type radical anions α- or β- to unsaturation.[2] The unsaturated group of the substrate usually acts as a captor during the primary act of electron transfer. The electron then migrates intramolecularly to a σ^* part of the substrate, which is activated toward dissociation. When dealing with complex molecules, interesting problems on intramolecular selectivity of cleavage and cleavage rates appear after electron attachment.[10]

A specially intriguing case was reported by Maslak and Guthrie.[11] They found that the C−O σ fragmentation of the radical anions of 4-nitrobenzyl phenyl ethers de-

(1) Balzani, V. *Electron Transfer in Chemistry*; Wiley-VCH Verlag GmbH: Weinheim, 2001; Vol. 5.
(2) Chanon, M.; Rajzmann, M.; Chanon, F. *Tetrahedron* **1990**, *46*, 6193.
(3) (a) Maslak, P.; Narvaez, J. N.; Vallombroso, T. M., Jr. *J. Am. Chem. Soc.* **1995**, *117*, 12373. (b) Maslak, P.; Narvaez, J. N. *Angew. Chem., Int. Ed. Engl.* **1990**, *29*, 283.
(4) Rossi, R. A.; Pierini, A. B.; Peñéñory, A. B. *Chem. Rev.* **2003**, *103*, 71.
(5) (a) Savéant, J.-M. *Tetrahedron* **1994**, *50*, 10117 (b) Maslak, P. *Top. Curr. Chem.* **1993**, *168*, 1 (c) Sancar, A. *Biochemistry* **1994**, *33*, 2.
(6) Pisano, L.; Farriol, M.; Asensio, X.; Gallardo, I.; González-Lafont, A.; Lluch, J. M.; Marquet, J. *J. Am. Chem. Soc.* **2002**, *124*, 4708.
(7) Pierini, A. B.; Vera, D. M. A. *J. Org. Chem.* **2003**, *68*, 9191.
(8) Laage, D.; Burghardt, I.; Sommerfeld, T.; Hynes, J. T. *Chem. Phys. Chem.* **2003**, *4*, 61.
(9) Laage, D.; Burghardt, I.; Sommerfeld, T.; Hynes, J. T. *J. Phys. Chem. A* **2003**, *107*, 11271.
(10) (a) Azzena, U.; Denurra, T.; Melloni, G. *J. Org. Chem.* **1992**, *57*, 1444. (b) Azzena, U.; Melloni, G.; Pisano, L. *Tetrahedron Lett.* **1993**, *34*, 5635.
(11) Maslak, P.; Guthrie, R. D. *J. Am. Chem. Soc.* **1986**, *108*, 2628.

10.1021/jo040208t CCC: $30.25
Published on Web 12/23/2004

SCHEME 1

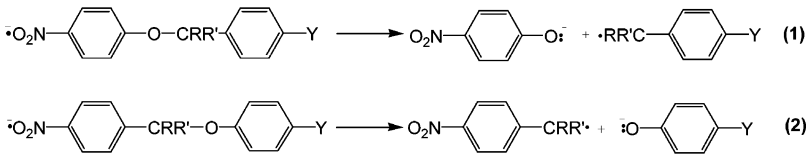

scribed by eq 2 took place at least 10^4 times faster in Me_2SO or tetrahydrofuran than the fragmentation of the corresponding 4-nitrophenyl benzyl ethers according to eq 1, despite the greater thermochemical driving force for the latter set of reactions (see Scheme 1). While the reaction of eq 2 may be viewed as an essentially heterolytic process involving transfer of charge across the C−O scissile bond, the reaction of eq 1 is formally a homolytic process, with the charge remaining localized in the original moiety. Maslak and Guthrie proposed the inherent preference for radical anion scission reactions occurring with regioconservation of spin density, i.e., where the unpaired electron remains on the same side of the scissile bond throughout the fragmentation process. This preference was interpreted in terms of σ-bond polarization at the transition state.[7,11] Thus, Maslak and Guthrie offered the hypothesis that the transition state for eq 2 can be approximated by a bond-polarized structure $^{-\bullet}NO_2C_6H_4CRR'^{+-}:OC_6H_5$, which is clearly lower in energy than any bond-polarized representation of the transition state for eq 1, like $^{-\bullet}NO_2C_6H_4O^{+-}:CRR'C_6H_5$ or $^{-\bullet}NO_2C_6H_4O^{-}:{}^{+}CRR'C_6H_5$. The same authors[12] obtained similar results by replacing the nitrophenyl moiety with a naphthyl group in eqs 1 and 2. Later, Guthrie and Shi[13] studied the reactions of (1-naphthyl)methyl phenyl ether and 1-naphthyl benzyl ether, in competition against the corresponding naphthalene-ring-deuterated or benzyl-deuterated compounds, with one-electron donors as fluoranthene radical anion. From their results they suggested that the transition state for the heterolytic cleavage resembles, to some extent, the π radical anion from which it comes, whereas the transition state for the homolytic cleavage is best viewed as a σ^* radical anion, wherein the extra electron is largely localized in the C−O σ bond with some minor delocalization into the benzene ring.

A quantitative comparison of the two cleavage modes for mesolysis of C−S σ bonds has been done by Maslak and Theroff[14] by replacing the C−O scissile bond in eqs 1 and 2 by a C−S bond. They found that the intrinsic barriers in DMF of the homolytic fragmentation are substantially higher (by ca. 3 kcal/mol) than those of the heterolytic cleavage.

Recently, we have studied[6] the mesolytic fragmentation of radical anions of 4-cyanophenyl benzyl ether and 4-cyanobenzyl phenyl ether, both electrochemically and theoretically. These two reactions correspond to eqs 1 and 2, respectively, with R = R′ = H, having replaced the nitro group by a cyano group. The electrochemical results indicated that the Gibbs free energy barrier in DMF at room temperature for the heterolytic fragmentation is 2.8 kcal/mol lower than the corresponding value for the homolytic process. The theoretical calculations in gas

SCHEME 2

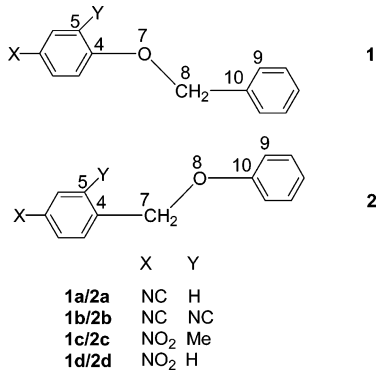

	X	Y
1a/2a	NC	H
1b/2b	NC	NC
1c/2c	NO_2	Me
1d/2d	NO_2	H

phase within the density functional theory (DFT) framework have reproduced quite well the experimental difference in free energy barriers, showing that the introduction of the cyano substituent favors thermodynamically the homolytic cleavage, but it favors kinetically the heterolytic fragmentation.

In this paper, we exten the above-mentioned theoretical study to three additional pairs of homolytic/heterolytic C−O aniomesolytic fragmentations in the gas phase, analogous to those in eqs 1 and 2, with the purpose of understanding the main factors that determine the relative rates of these kind of aniomesolytic cleavages. In particular, we compare (see Scheme 2) the homolytic fragmentations of the radical anions of 4-cyanophenyl benzyl ether (**1a**), 2,4-dicyanophenyl benzyl ether (**1b**), 2-methyl-4-nitrophenyl benzyl ether (**1c**), and 4-nitrophenyl benzyl ether (**1d**) with the heterolytic fragmentations of the radical anions of 4-cyanobenzyl phenyl ether (**2a**), 2,4-dicyanobenzyl phenyl ether (**2b**), 2-methyl-4-nitrobenzyl phenyl ether (**2c**), and 4-nitrobenzyl phenyl ether (**2d**).

2. Method of Calculation

DFT has been used to carry out the electronic structure calculations. The spin-unrestricted formalism has been employed in solving the Kohn−Sham DFT equations.[15] The particular functional chosen has been the Becke's three-parameter hybrid method with the Lee, Yang, and Parr correlation functional (B3LYP).[16] This functional has already been used successfully by several authors to study similar aromatic systems.[6,7,17,18] Unless it is said otherwise, the split-valence 6-31+G basis set,[19] which

(12) Maslak, P.; Guthrie, R. D. *J. Am. Chem. Soc.* **1986**, *108*, 2637.
(13) Guthrie, R. D.; Shi, B. *J. Am. Chem. Soc.* **1990**, *112*, 3136.
(14) Maslak, P.; Theroff, J. *J. Am. Chem. Soc.* **1996**, *118*, 7235.
(15) (a) Hohenberg, P.; Kohn, W. *Phys. Rev. B* **1964**, *136*, 864. (b) Kohn, W.; Sham, L. J. *Phys. Rev. A* **1965**, *140*, 1133.
(16) (a) Lee, C.; Yang, W.; Parr, R. G. *Phys. Rev. B* **1988**, *37*, 785. (b) Becke, A. D. *J. Chem. Phys.* **1993**, *98*, 5648.
(17) Pratt, D. A.; de Heer, M. I.; Mulder, P.; Ingold, K. U. *J. Am. Chem. Soc.* **2001**, *123*, 5518.
(18) Dem'yanov, P. I.; Myshakin, E. M.; Boche, G.; Petrosyan, V. S.; Alekseiko, L. N. *J. Phys. Chem. A* **1999**, *103*, 11469.
(19) Clark, T.; Chandrasekhar, J.; Spitznagel, G. W.; Shleyer, P. v. R. *J. Comput. Chem.* **1983**, *4*, 294.

includes a diffuse sp shell on the heavy atoms, has been employed throughout this paper. In some cases, single-point energy calculations at the B3LYP/6-31+G(d)//B3LYP/6-31+G level have been carried out with the split valence 6-31+G(d) basis set[20] which includes polarization functions on the heavy atoms.

Full geometry optimization and direct location of stationary points have been done with the Schlegel gradient optimization algorithm by using redundant internal coordinates.[21] The characterization of the stationary points, minima, or transition-state structures, has been carried out by diagonalizing their analytical second-derivative matrix (Hessian) and looking for zero or one negative eigenvalue, respectively. In this second case, the eigenvector (transition vector) associated to the negative eigenvalue shows the direction along which the potential energy lowers.

Thermodynamic and quasi-thermodynamic magnitudes have been computed using the statistical thermodynamic formulation[22] of partition functions within the ideal gas, rigid rotor, and harmonic oscillator models. Analytical second derivatives of the energy with respect to the Cartesian coordinates have been used for the determination of vibrational frequencies. The imaginary frequency is neglected in the thermodynamic calculations of the transition-state structures. A pressure of 1 atm and a temperature of 298.15 K have been assumed in the calculations.

A natural population analysis (NPA) according to the procedure developed by Weinhold and co-workers has been done to obtain the net charges and the spin distribution (the difference between the α and the β NPA net atomic charges, that is, the α spin excess).[23]

In some cases, the bulk effect of a polar solvent has been evaluated through the Tomasi's polarized continuum model (PCM)[24] at the gas-phase geometry. A dielectric constant value of 36.64 corresponding to acetonitrile has been used.

All of the calculations have been performed with the Gaussian 98 program package.[25]

3. Results and Discussion

First we will present the results corresponding to the C−O alkyl ether homolytic mesolytic bond fragmentations of radical anions **1a**−**1d**. Second, we will analyze the corresponding heterolytic mesolytic bond fragmentations of radical anions **2a**−**2d**, focusing on the most relevant differences between the two kind of cleavages.

For each homolytic mesolytic cleavage of radical anions **1a**−**d** we have located several stationary points on the corresponding potential energy surfaces. Their main geometrical parameters (the C−O distance of the scissile bond and the three dihedral angles that indicate the relative twisting of the two aromatic rings), relative potential energy (without zero-point energy), and Gibbs free energy are shown in Table 1. The geometrical parameters of the corresponding neutral molecules are also included for the sake of comparison. The numbers labeling the atoms are indicated in Scheme 2.

The two aromatic rings of the neutral species corresponding to the radical anions **1a**−**d** lie on the molecular plane. After the electron is captured, several minima exist with a C−O alkyl ether bond distance close to the value in the neutral structure. In each case (**1a**−**d**), the most stable structure in terms of potential energy is the one which keeps that planar geometry and has the shortest C−O bond. This structure will be called from here on radical anion and it will be considered as the reactant for the C−O bond fragmentation. The other minima, also included in Table 1, have somewhat longer C−O distances, and their aromatic rings have turned away from the molecular plane. That is, these other minima are higher energy conformers of the corresponding radical anions and they will not be taken into account because the reaction paths go directly from each radical anion to the corresponding transition-state structure. Then, the energy barriers will be taken from the radical anions.

The NPA net atomic charges and spin distributions for the radical anions **1a**−**d** and their corresponding transition-state structures are shown in Table 2 (see also the Supporting Information, Table 56, for more information). The added electron mainly goes to the π system in the radical anion (to a π radical anion molecular orbital which comes from the π^* molecular orbital of the neutral species). In **1a** it is mainly distributed among the phenyl ring, the cyano group attached to it, and the benzyl ring, whereas in **1b** the presence of the two cyano groups in the same ring localizes the unpaired electron in the phenyl ring, with some participation of the cyano groups. Due to its stronger withdrawing character, the nitro group collects most of the added electron in **1c** and **1d**, although part of the electron still lies in the phenyl ring. Interestingly, the C−O scissile bond is slightly shorter (about 0.02 Å) in the radical anion than in the corresponding neutral species (see Table 1). This fact can be understood noting that the oxygen atom, which is directly linked to the phenyl ring of the side that supports the extra electron, has a very small (0.013−0.014 au), but non-negligible, α spin excess in the radical anion (Table 2). As is well-known, in a C−O bond the main contribution to the bonding σ molecular orbital comes from the oxygen atom, whereas the carbon atom provides the most important contribution to the antibonding σ^* molecular orbital. Then, it can be thought that the extra electron contributes to slightly increase the population of the σ C−O alkyl ether bond, this way reinforcing the bond strength and shortening it.

(20) Pople, J. A.; Frisch, M. J.; Luke, B. T.; Binkley, J. S. *Int. J. Quantum Chem., Symp.* **1983**, *17*, 307.
(21) Peng, C.; Ayala, P. Y.; Schlegel, H. B.; Frisch, M. J. *J. Comput. Chem.* **1996**, *17*, 49.
(22) McQuarrie, D. A. *Statistical Thermodynamics*; University Sciences Books: Mill Valley, CA, 1973.
(23) (a) Reed, A. E.; Weinstock, R. B.; Weinhold, F. *J. Chem. Phys.* **1985**, *83*, 735 (b) Reed, A. E.; Curtiss, L. A.; Weinhold, F. *Chem. Rev.* **1988**, *88*(8), 899.
(24) Miertus, S.; Scrocco, E.; Tomasi, J. *Chem. Phys.* **1981**, *55*, 117.
(25) Frisch, M. J.; Trucks, G. W.; Schlegel, H. B.; Scuseria, G. E.; Robb, M. A.; Cheeseman, J. R.; Zakrzewski, V. G.; Montgomery, J. A.; Stratmann, R. E.; Burant, J. C.; Dapprich, S.; Millam, J. M.; Daniels, A. D.; Kudin, K. N.; Strain, M. C.; Farkas, O.; Tomasi, J.; Barone, V.; Cossi, M.; Cammi, R.; Mennucci, B.; Pomelli, C.; Adamo, C.; Clifford, S.; Ochterski, J.; Petersson, G. A.; Ayala, P. Y.; Cui, Q.; Morokuma, K.; Malick, D. K.; Rabuck, A. D.; Raghavachari, K.; Foresman, J. B.; Cioslowski, J.; Ortiz, J. V.; Stefanov, B. B.; Liu, G.; Liashenko, A.; Piskorz, P.; Kamaromi, I.; Gomperts, R.; Martin, R. L.; Fox, D. J.; Keith, T.; Al-Laham, M. A.; Peng, C. Y.; Nanayakkara, A.; Gonzalez, C.; Challacombe, M.; Gill, P. M. W.; Johnson, B. G.; Chen, W.; Wong, M. W.; Andres, J. L.; Head-Gordon, M.; Replogle, E. S.; Pople, J. A. *Gaussian 98*, revision A7; Gaussian Inc.: Pittsburgh, PA, 1998.

TABLE 1. Main Geometrical Parameters of the Stationary Points Located for the C−O Alkyl Ether Homolytic Bond Fragmentation of the Radical Anions 1a−d along with the Corresponding Potential Energies and Gibbs Free Energies. Neutral Structures Are Also Included

	O_7C_8 [a]	$C_5C_4O_7C_8$ [b]	$C_4O_7C_8C_{10}$ [b]	$O_7C_8C_{10}C_9$ [b]	ΔV[c]	$\Delta G°$ [c]
1a						
neutral species	1.460	180.0	180.0	0.0		
radical anion	1.441	180.0	180.0	0.0	0	0
minimum	1.446	177.3	−78.5	12.9	1.50	1.03
TS	1.481	129.5	−64.6	−40.5	2.41	1.21
complex	3.233	1.1	180.7	0.0	−29.1	−33.4
products	∞				−21.7	−34.3
1b						
neutral species	1.464	180.0	180.0	0.0		
radical anion	1.440	180.0	180.0	0.0	0	0
minimum 1	1.445	−171.9	−82.1	−17.1	1.66	1.40
minimum 2	1.454	138.8	−70.1	−33.4	2.62	1.86
TS	1.547	82.2	−8.73	−103.2	4.58	4.55
complex	3.382	−179.7	179.7	0.0	−24.7	−28.4
products	∞				−18.2	−31.4
1c						
neutral species	1.462	180.0	180.0	0.0		
radical anion	1.441	180.0	180.0	0.0	0	0
minimum 1	1.459	98.7	177.3	171.5	0.33	−0.42
minimum 2	1.484	118.3	−77.8	83.9	1.22	0.78
TS	1.901	106.4	−79.4	89.5	9.94	7.76
complex	3.303	−179.9	−179.2	0.02	−6.43	−12.2
products	∞				0.84	−14.6
1d						
neutral species	1.463	180.0	180.0	0.0		
radical anion	1.441	180.0	180.0	0.0	0	0
minimum 1	1.460	82.8	−177.8	8.0	0.28	−0.73
minimum 2	1.485	110.7	−78.7	−90.4	1.23	0.88
TS	1.921	97.3	−78.8	−86.5	10.4	7.98
complex	3.295	−0.3	179.9	0.0	−5.29	−9.28
products	∞				0.82	−12.8

[a] Bond distances in angstroms. [b] Dihedral angles in degrees. [c] In kcal/mol.

An intramolecular electron transfer to the σ^* molecular orbital of the C−O bond is required to produce the bond dissociation. However, for symmetry reasons, there is no $\pi-\sigma^*$ electronic coupling in a planar geometry. The π and σ^* states become coupled when a symmetry-breaking coordinate motion occurs, thus making the intramolecular electron transfer feasible. In the present case, this symmetry-breaking motion consists of the twisting of the two aromatic rings. The scissile C−O bond stretching due to random thermal fluctuations leads from the radical anion to the transition-state structure (TS), which is reached when a significant α spin excess (0.031−0.310 au) is accumulated in the carbon atom of that C−O bond (see Table 2). This spin distribution indicates some electron population in the σ^* C−O molecular orbital. As indicated by the corresponding dihedral angles in Table 1, in all the transition-state structures the two aromatic rings have twisted in order to make possible the $\pi-\sigma^*$ electronic coupling. The transition vectors consist mostly of the variation of the scissile C−O bond distance plus some components corresponding to the twisting of those dihedral angles. The migration of the electron density from the π region in the phenyl moiety of the molecule to the σ^* C−O region (whose main contribution corresponds to the carbon atom, already in the benzyl moiety of the molecule) is more difficult as the electron-withdrawing strength of the substituents attached to the phenyl ring increases. Thus, as seen in Table 1, in going from **1a** (with a cyano group attached to the phenyl ring) to **1d** (with a nitro group attached to the phenyl ring) the C−O bond distance at the transition-state structure (from 1.481 to 1.921 Å), the potential energy barrier (from 2.41 to 10.4 kcal/mol), and the free energy barrier (from 1.21 to 7.98 kcal/mol) increase monotonically. As expected, one nitro group has a stronger influence than two cyano groups, whereas one methyl group facilitates the migration of the electron density toward the σ^* C−O region. Note that the favorable contribution of the entropic term to the fragmentation process is due to the fact that, relative to the radical anion, the free energies are lower than the corresponding potential energies, the difference tending to increase as the cleavage advances. Thus, the entropy change lowers the barrier, facilitating the fragmentation. Each transition-state structure dissociates through a complex, where the C−O scissile bond is already broken (it is longer than 3.2 Å), composed by two fragments: a closed-shell substituted phenolate anion which supports roughly one negative net charge, and an almost neutral benzyl radical which contains an entire unpaired α electron. From here the products are reached with a cost of 6−7 kcal/mol in terms of potential energy, but with a small loss of free energy. All the cleavages are exergonic, although the driving force diminishes from **1a** to **1d**. This trend is mainly because most of the negative net charge in the complexes and in the products lies on the oxygen atom, with a parallel diminution on the phenyl ring and their substituents. This change is more difficult as the electron-withdrawing character of those substituents grows.

The C−O bond distance for the **1a** transition-state structure turns out to be very short. To verify that it is actually the transition-state structure corresponding to

TABLE 2. NPA Net Atomic Charges (in au) and Spin Distribution (in au) for the Radical Anions 1a−d and Their Corresponding Transition-State Structures

1a

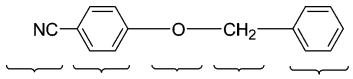

	A	A'	B	C	D
Radical anion (charge)	-0.238	-0.270	-0.554	0.295	-0.235
TS (charge)	-0.232	-0.264	-0.577	0.302	-0.228
Radical anion (spin)	0.183	0.583	0.013	0.000	0.224
TS (spin)	0.169	0.592	0.012	0.031	0.201

1b

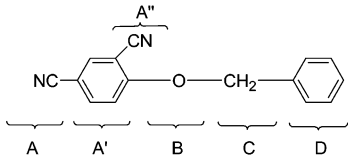

	A	A'	A"	B	C	D
Radical anion (charge)	-0.136	-0.379	-0.188	-0.545	0.314	-0.066
TS (charge)	-0.149	-0.287	-0.169	-0.586	0.298	-0.107
Radical anion (spin)	0.048	0.745	0.153	0.014	0.014	0.025
TS (spin)	0.074	0.658	0.124	-0.001	0.054	0.090

1c

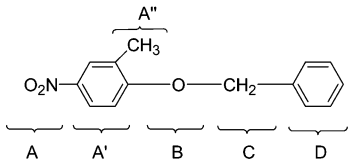

	A	A'	A"	B	C	D
Radical anion (charge)	-0.921	0.187	0.025	-0.561	0.324	-0.054
TS (charge)	-0.683	0.271	0.032	-0.613	0.191	-0.197
Radical anion (spin)	0.730	0.247	-0.001	0.014	0.004	0.006
TS (spin)	0.368	0.135	0.001	-0.022	0.296	0.221

1d

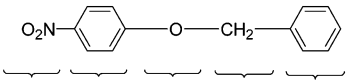

	A	A'	B	C	D
Radical anion (charge)	-0.919	0.209	-0.560	0.323	-0.053
TS (charge)	-0.685	0.297	-0.613	0.186	-0.185
Radical anion (spin)	0.728	0.249	0.014	0.004	0.005
TS (spin)	0.372	0.134	-0.030	0.310	0.213

the C−O bond fragmentation we have slightly moved that structure forward and backward along the direction associated to the transition vector, and then we have relaxed the corresponding geometries. As expected, the molecule evolves to the complex and the radical anion, respectively.

Let us turn now our attention to the heterolytic cleavage of radical anions **2a**−**d**. We will focus on the comparison with the corresponding homolytic fragmentations. Tables 3 and 4 collect the main results relative to geometries, energies, and NPA electron distribution of the located stationary points and are analogous to the previous Tables 1 and 2, respectively.

The two aromatic rings of the neutral species corresponding to the radical anions **2a**−**d** are on the molecular plane, except the benzyl ring of **2c**, which has to turn around the C_4C_7 bond in order to avoid the steric hindrance between the methyl and the methylene groups (see Table 3). Conversely to the homolytic case, when the electron is added no stationary point with a C−O alkyl ether bond distance shorter than in the neutral molecule exists. Instead, some stationary points with a C−O bond distance slightly longer than the value in the neutral species have been located. Again the most stable of those stationary points in terms of potential energy in each case (**2a**−**d**) will be called the radical anion. The radical anions **2a** and **2b** are planar. However, in the radical anions **2c** and **2d** the benzyl ring has turned around the C_4C_7 bond. The lesser trend of the radical anions **2** to be planar is probably due to the lack of conjugation between the π system that supports most of the added electron and the oxygen atom, in contrast to the conjugation present in the radical anions **1**.

The NPA net atomic charges and spin distributions for the radical anions **2a**−**d** and their corresponding transition-state structures are shown in Table 4 (see also Supporting Information, Table 57 for more information). As in the radical anions **1**, the extra electron mostly goes to the π system in the radical anions **2**. In **2a** and **2b** it mainly lies on the benzyl ring, with some participation of the cyano groups attached to it. The nitro group accumulates most of the added electron in **2c** and **2d**, although part of the electron still is in the benzyl ring. Note that the benzyl ring in all the radical anions **2** retains clearly more negative charge than the phenyl ring in the radical anions **1**, in which this phenyl ring is attached and conjugated to the oxygen atom. Conversely to the case of radical anions **1**, in the radical anions **2** the C−O alkyl ether bond is somewhat longer (0.0−0.06 Å) than in the corresponding neutral molecules (see Table 3). This is because now the atom of the C−O bond which is directly attached to the benzyl ring that supports the extra electron is the carbon atom, in such a way that it has some α spin excess (0.010−0.043 au) in the radical anions **2**. This indicates that the extra electron contributes to slightly augment the population of the σ^* molecular orbital corresponding to the C−O alkyl ether bond, so weakening and lengthening it.

The analysis of the eigenvalues of the Hessian matrixes shows that the radical anions **2c** and **2d** are minimum energy structures, but **2a** and **2b** are actually transition-state structures, whose transition vector is a mixture of the twisting of the dihedral angles that breaks the planarity of the molecule, but it does not contain any component corresponding to the elongation of the C−O alkyl ether bond. Thus, no minimum energy structures corresponding to the radical anions **2a** and **2b** exist. Due to the weak electron-withdrawing character of the cyano groups, the extra electron already populates the σ^* C−O molecular orbital in a non-negligible amount (the α spin excess in the carbon atom is 0.043 or 0.025 au in the radical anions **2a** and **2b**, respectively) for short C−O bond distances. Then the symmetry-breaking motions that couple the π and σ^* systems are enough to initiate the fragmentation. Radical anions **2a** and **2b** are minima along the direction corresponding to the C−O elongation, but maxima along the direction that twists the rings away from planarity. When their geometry is displaced some few degrees along this last direction and then allowed to relax, the C−O bond breaks leading to the corresponding complex. In other words, the intermolecular[26] electron transfer that provides the extra electron is dissociative for the heterolytic cleavages of **2a** and **2b**. Conversely, for the homolytic cleavages of **1a**−**d**, and the heterolytic cleavages of **2c** and **2d**, only the intramolecular[26] electron transfer is dissociative. So, as seen in Table 3, it can be considered that the transition-state structures

(26) Savéant, J.-M. In *Advances in Physical Organic Chemistry*; Tidwell, T. T., Ed.; Academic Press: New York, 2000; p 35.

TABLE 3. Main Geometrical Parameters of the Stationary Points Located for the C−O Alkyl Ether Heterolytic Bond Fragmentation of the Radical Anions 2a−d along with the Corresponding Potential Energies and Gibbs Free Energies. Neutral Structures Are Also Included

	C_7O_8 [a]	$C_5C_4C_7O_8$ [b]	$C_4C_7O_8C_{10}$ [b]	$C_7O_8C_{10}C_9$ [b]	ΔV[c]	ΔG° [c]
2a						
neutral species	1.451	0.0	180.0	180.0		
radical anion (TS)	1.468	0.0	180.0	180.0	0	0
complex	2.642	89.0	175.4	89.8	−13.1	−16.0
products	∞				−0.6	−13.8
2b						
neutral species	1.438	0.0	180.0	180.0		
radical anion (TS)	1.456	0.0	180.0	180.0	0	0
complex	3.042	180.0	179.5	0.9	−13.8	−17.9
products	∞				10.3	−3.61
2c						
neutral species	1.467	−71.81	179.5	179.7		
radical anion	1.512	80.5	−179.5	179.2	0	0
minimum	1.538	104.7	−63.4	74.9	2.54	2.33
TS	2.847	113.7	−30.2	−91.4	12.3	7.15
complex	3.040	180.0	179.9	0.2	10.6	5.79
products	∞				32.1	17.3
2d						
neutral species	1.450	0.0	180.0	180.0		
radical anion	1.509	114.2	177.6	−178.0	0	0
minimum	1.532	105.9	−67.6	73.9	1.55	1.15
TS	2.817	124.5	−65.2	94.0	13.1	8.02
complex	3.036	−0.2	177.8	−177.4	11.1	6.41
products	∞				33.3	19.2

[a] Bond distances in angstroms. [b] Dihedral angles in degrees. [c] In kcal/mol.

for the **2a** and **2b** fragmentations appear at the C−O values of 1.468 and 1.456 Å, respectively, with no energy barrier. Instead, the presence of the nitro group in **2c** and **2d** delays the appearance of the corresponding transition-state structures (C−O bond distances of 2.847 and 2.817 Å, respectively), with high potential energy barriers (12.3 and 13.1 kcal/mol, respectively) and free energy barriers (7.15 and 8.02 kcal/mol, respectively) somewhat attenuated due to the entropic contribution. The transition vectors of these two last transition-state structures, in which two aromatic rings are clearly twisted, consist of a mixture of the elongation of the C−O bond and the twisting of the dihedral angles. The α spin excess in the carbon atom of the C−O bonds is 0.326 au in both cases. Very interestingly, in terms of potential energy barriers the heterolytic fragmentations are faster than the corresponding homolytic ones for the **a** and **b** cases but slower for the **c** and **d** cases. The entropic contribution makes comparable the homolytic and heterolytic free energy barriers for **c** and **d**. Each transition-state structure dissociates through a complex, where the C−O alkyl ether bond is already broken (it is longer than 2.6 Å), composed by two fragments: a substituted benzyl radical which still keeps some of the original negative net charge and that contains most of the unpaired α electron and a phenolate anion which supports most of the negative net charge and still has some radical character. From here the products are reached with an important cost both in terms of potential energy (from 12.5 to 24.1 kcal/mol) and in terms of free energy (from 2.2 to 14.3 kcal/mol). The cleavages of radicals **2a** and **2b** are exergonic, whereas the fragmentations of **2c** and **2d** turns out to be endergonic, as a consequence of the difficulty for transferring the extra electron from the moiety containing the increasingly powerful electron withdrawing groups to the other moiety. As expected, the homolytic fragmentations, where the negative net charge remains in the moiety containing the electron withdrawing groups, are thermodinamically very favored versus the corresponding heterolytic ones.

To test the influence of the inclusion of polarization functions in the basis set, we have carried out single-point energy calculations at the B3LYP/6-31+G(d)//B3LYP/6-31+G level to recalculate the potential energy barriers of the different fragmentations. The new barriers (see the Supporting Information, Table 58) turn out to be quite close to the B3LYP/6-31+G barriers already shown in Tables 1 and 3, so confirming the main trends of the fragmentation reactions discussed so far.

At this point, a qualitative discussion in terms of valence bond electronic configurations can be useful. For the sake of simplicity, let us compare the cleavage of radical anions **a** (supporting one cyano grup) and **d** (containing one nitro group), which are the two extremes of the series studied here. As we will see below, we think that the relevant configurations in each region of the potential energy surface depends mainly on the strength of the electron-withdrawing substituents, although the relative weight of each configuration change somewhat from the homolytic to the heterolytic case. In Table 5 we have listed the configurations we need for the discussion.

Underscripts 1 and 2 label the configurations corresponding to the homolytic and heterolytic fragmentations, respectively. The suitable combination of these configurations explains the NPA net atomic charges and spin distribution shown in Tables 2 and 4 (and Tables 56 and 57 of the Supporting Information). Configurations A_1, B_1, and C_1 correspond to the extra electron localized in the electron-withdrawing substituent (X = −CN or $-NO_2$), the phenyl group, and the benzyl group, respectively. The radical anion **1a** involves a mixture of those three configurations, B_1 having the most important weight (α spin excess of 0.583 au in the phenyl group). The transition-state structure of **1a** adds D_1 to those three

TABLE 4. NPA Net Atomic Charges (in au) and Spin Distribution (in au) for the Radical Anions 2a−d and Their Corresponding Transition-State Structures

2a

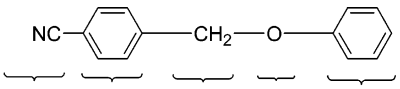

	A	A'	B	C	D
Radical anion (TS) (charge)	-0.236	-0.576	0.299	-0.544	0.062
Radical anion (TS) (spin)	0.183	0.650	0.043	-0.001	0.125

2b

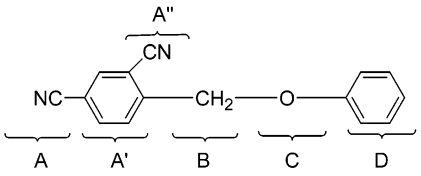

	A	A'	A"	B	C	D
Radical anion (TS) (charge)	-0.184	-0.622	-0.141	0.300	-0.524	0.171
Radical anion (TS) (spin)	0.128	0.743	0.088	0.025	0.000	0.015

2c

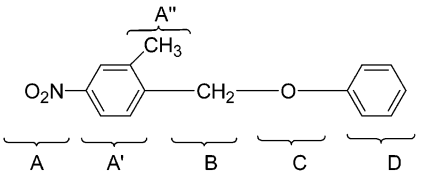

	A	A'	A"	B	C	D
Radical anion (charge)	-0.871	-0.055	0.014	0.296	-0.539	0.156
TS (charge)	-0.559	0.048	0.030	0.146	-0.699	0.034
Radical anion (spin)	0.676	0.294	0.001	0.010	0.017	0.003
TS (spin)	0.153	0.192	0.004	0.326	0.189	0.136

2d

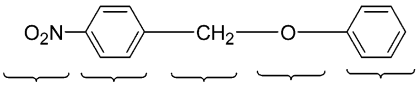

	A	A'	B	C	D
Radical anion (charge)	-0.870	-0.044	0.296	-0.537	0.155
TS (charge)	-0.561	0.076	0.142	-0.691	0.034
Radical anion (spin)	0.675	0.296	0.010	0.016	0.003
TS (spin)	0.159	0.187	0.326	0.201	0.127

TABLE 5. Relevant Electronic Configurations for the Cleavage of Radical Anions a−d[a]

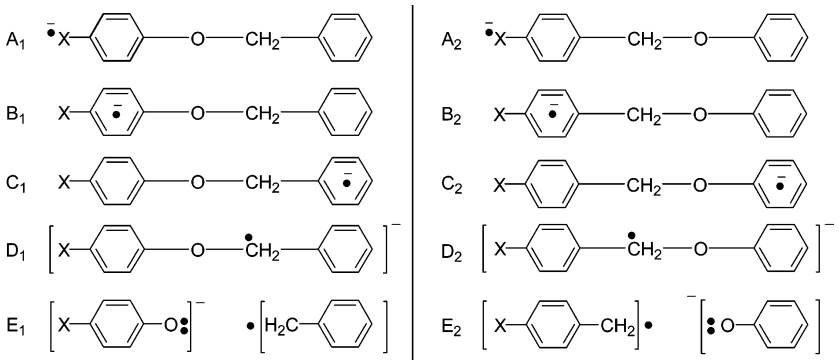

[a] X stands for the electron-withdrawing substituents (−CN or $-NO_2$). Subscripts 1 and 2 label the configurations corresponding to the homolytic and heterolytic fragmentations.

configurations, B_1 still being the dominant (α spin excess of 0.592 au in the phenyl group). D_1 is the result of the intramolecular electron transfer between the π system and the σ^* molecular orbital corresponding to the C−O alkyl ether bond. The small contribution of D_1 produces an α spin excess in the carbon atom of 0.031 au. In the configuration E_1 the C−O bond is already broken, the negative charge is in the cyanophenolate anion (mainly in the oxygen atom), and the unpaired electron lies in the benzyl radical (mainly in the carbon atom). Indeed, the products of the homolytic fragmentation of **1a** are defined by the configuration E_1. The configurations labeled with the underscript 2 are analogous to the ones described above, but for the heterolytic cleavage. So, the radical anion−transition-state structure **2a** involves the configurations A_2, B_2, C_2, and D_2, the configuration B_2

being the dominant (α spin excess of 0.650 and 0.043 au in the benzyl ring and the carbon atom, respectively). The small contribution of D_2 (or D_1) is the distinctive feature of the transition-state structure of the heterolytic (or homolytic) cleavage of the cyano-substituted compounds **a**. Kinetics in this case depends on the configurations D, that is, on the cost to produce the migration of the added electron to the C−O σ^* molecular orbital. The farther away from the cyano group the migration, the bigger the potential energy barrier. As a consequence, D_2 is lower than D_1, explaining why the heterolytic fragmentation of **2a** is faster than the homolytic fragmentation of **1a**. On the other hand, E_2 is the configuration of the products of the heterolytic fragmentation of **2a**. So, thermodynamics of the cleavage of the cyano substituted compounds **a** depends on the configurations E (nothing to do with the configurations D which determine the kinetics). Because of the stabilizing effect of the electron-withdrawing cyano substituent in the products, which is clearly larger in the cyanophenolate anion than in the cyanobenzyl radical, E_1 is lower than E_2, this way explaining why the homolytic fragmentation is the thermodinamically favored.

The scenario for the radical anions **d** is different. The radical anion **1d** is described by the configurations A_1 (the largely dominant: α spin excess of 0.728 au in the nitro group) and B_1. The transition-state structure includes important contributions of A_1 and E_1 (α spin excess of 0.372 au and 0.310 au in the nitro group and the carbon atom of the scissile C−O bond, respectively) and some participation of B_1. The corresponding products are defined by the configuration E_1. In turn, the radical anion **2d** is described by the configurations A_2 (the largely dominant: α spin excess of 0.675 au in the nitro group) and B_2. The transition-state structure includes contributions of A_2, B_2, and mainly E_2 (α spin excess of 0.326 au in the carbon atom of the scissile C−O bond). The contribution of E_2 (or E_1) is the distinctive feature of the transition-state structure of the heterolytic (or homolytic) cleavage of the nitro-substituted compounds **d**. Kinetics in this case depends on the configurations E. On the other hand, E_2 is the configuration of the products of the heterolytic fragmentation of **2d**. Thus, both kinetics and thermodynamics of the fragmentation of the nitro-substituted compounds **d** depends on the configurations E. Due to the strong electron-withdrawing character of the nitro group, E_1 is lower than E_2, and this explains why the homolytic fragmentation of radical anions **d** is more favored than the heterolytic one in terms of potential energy both kinetically and thermodinamically. Compounds **b** and **c** lie between **a** and **d** along the series **a**−**d**, the behavior of **b** being similar to that of **a** and the behavior of **c** being close to that of **d**.

At this point, our prediction that the homolytic fragmentation of the nitro radical anions **d** is faster than the corresponding heterolytic one can seem surprising and contrary to the experimental results. However, this prediction is in terms of potential energy. The transition-state structures for cleavages of **1d** and **2d** appear at C−O alkyl ether distances of 1.921 and 2.817 Å, respectively (see Tables 1 and 3). Then, as said above, the entropic contribution (which here favors the later transition-state structure) makes comparable the homolytic and heterolytic free energy barriers, 7.98 and 8.02 kcal/mol, respectively. On the other hand, all of the theoretical results presented in this paper correspond to the gas phase. It is expected that the heterolytic fragmentation becomes faster in a polar solvent. This assumption is based on the fact that the rate of fragmentation of radical anions **d** depends on the electronic configurations corresponding to the products E_1 and E_2. In the gas phase, the thermodynamic reaction values of ΔV and $\Delta G°$ for the homolytic cleavage of **1d** are 0.82 and −12.8 kcal/mol, respectively. The corresponding values for the heterolytic cleavage of **2d** are 33.3 and 19.2 kcal/mol, respectively. PCM calculations, including both electrostatic and nonelectrostatic terms, give reaction energies in acetonitrile of 3.59 and 22.5 kcal/mol for **1d** and **2d**, respectively. Note that the difference between both fragmentations is noticeably reduced in going from the gas phase to the polar solvent. Taking into account the difference between ΔV and $\Delta G°$ in the gas phase, the reaction free energies in acetonitrile can be estimated to be −10.03 kcal/mol for **1d** and 8.4 kcal/mol for **2d**. It is clear that the presence of a polar solvent mainly stabilizes the heterolytic products. This is because the negative net charge of the phenolate anion is more localized in E_2 than in E_1. A similar effect will take place in the heterolytic transition-state structure. Our results suggest that the heterolytic fragmentation of the radical anion **2d** is experimentally faster than the homolytic cleavage of **1d** due not to pure electronic reasons, but to the effect of the polar solvent.

In light of the results presented here, another possibility that must be taken into account to explain the experimental results described in the literature[11] for the nitro cases in polar solvents would be the operation of dianions instead of radical monoanions as active species producing the C−O cleavages. This would therefore make the fragmentations more exergonic, and their expected behavior should be similar to the one described here for the cyano derivatives **a** and **b**. This is just what is experimentally observed.

4. Conclusions

We have carried out density functional theory electronic structure calculations to study the homolytic/heterolytic aniomesolytic C−O fragmentations in gas phase of a series of radical anions of substituted-phenyl benzyl ethers and substituted-benzyl phenyl ethers. Along the series, the electron-withdrawing strength of the substituents increases. The extra electron goes to the π system in the radical anion, mainly to the moiety containing the electron-withdrawing group. An intramolecular electron transfer to the σ^* molecular orbital of the scissile C−O bond is required to produce the fragmentation. This C−O bond lengthens to diminish the energy of the σ^* antibonding molecular orbital in order to make possible the intramolecular electron transfer. This electron migration becomes more difficult as the electron-withdrawing power of the substituents increases. As a consequence, the greater the electron-withdrawing strength of the substituents, the later the transition-state structures and the higher the potential energy barriers and the Gibbs free energy barriers.

As for the homolytic/heterolytic competition, the homolytic cleavages, in which the negative net charge keeps

in the moiety containing the electron-withdrawing groups, are always thermodynamically favored versus the corresponding heterolytic ones. The scenario for the kinetics turns out to be clearly different. Radical anions containing only weak electron-withdrawing groups (i.e., the cyano group) have early transition-state structures, whose location and barriers depends on a electronic configuration which is the result of the intramolecular electron transfer between the π system and the σ^* antibonding molecular orbital corresponding to the C−O alkyl ether bond. In this case, the heterolytic fragmentations, which involve a shorter migration of the electron density from the π system, are faster than the homolytic ones. Conversely, radical anions supporting strong electron-withdrawing groups (i.e., the nitro group) have late transition-state structures, which are already characterized by the same electron configuration as the products. Then, in terms of potential energy barriers, the homolytic fragmentations are faster. However, the entropic contribution, which favors the later transition-state structure, makes it comparable to the homolytic and the heterolytic Gibbs free energy barriers in this case.

This way, in the gas phase the energetic crossing, where the thermodinamically more favorable cleavage is the kinetically slower one, only occurs for radical anions with early transition-state structures. No crossing happens when strong electron-withdrawing substituents lead to late transition-state structures. Then, the spin regioconservation principle does not actually hold in some cases, and even when it seems to hold, it is not the real cause of the kinetic behavior of those radical anions. Finally, it should be remarked that the experimental results obtained with nitrosubstituted ethers[11] in polar solvents (heterolytic fragmentation the faster process) cannot be justified on electronic grounds. Two possibilities can be advanced: a solvent effect or the operation of dianions as the key active species.

Acknowledgment. We are grateful for financial support from the Spanish "Ministerio de Ciencia y Tecnología" and the "Fondo Europeo de Desarrollo Regional" through Project No. BQU2002-00301 and the use of the computational facilities of the CESCA.

Supporting Information Available: Tables 1−55 show the geometries, energies, and number of imaginary vibrational frequencies of the stationary points located. Tables 56 and 57 provide the NPA net atomic charges and spin distribution for the radical anions and related structures. Table 58 gives the B3LYP/6-31+G(d)//B3LYP/6-31+G potential energy barriers. Figures 1 and 2 provide spin density diagrams of several structures. This material is available free of charge via the Internet at http://pubs.acs.org.

JO040208T